Fermilab

Fermi National Accelerator Laboratory
P.O. Box 500 • Batavia, Illinois • 60510

TD – 02 – 025
May 15, 2002

Nb_3Sn Cos(θ) Dipole Magnet, HFDA-04 Production Report

D. R. Chichili[1], N. Andreev[1], E. Barzi[2], S. Bhashyam[1], V. Kashikhin[1], V. Kashikhin[2], I. Novitski[1], I. Terechkine[1], S. Yadav[1], R. Yamada[2], and A.V. Zlobin[2]

[1]Engineering and Fabrication Department
[2]Development and Test Department
Technical Division
Fermilab, Batavia, IL 60510

1.0 INTRODUCTION

HFDA-04 is the fourth Nb_3Sn shell-type magnet to be fabricated and the third to be tested. The dipole model is a 1 m long magnet with 43.5 mm bore aperture. Fig. 1 shows the completed magnet ready to be tested. Except for the coil end-saddle, the design of the magnet is similar to that of HFDA-03[1]. The coil winding and curing procedures were similar to that of the previous magnets. However, the reaction, splicing and impregnation procedures have been changed.

Fig. 1: *Photograph of HFDA-04 ready to be shipped to VMTF*

The specific features of HFDA-04 are listed below:

- The end-saddle was redesigned so that the lead cable comes out in the mid-plane. The entire splice joint now sits in the end-saddle and is well supported at all stages of the magnet operation. See Section – 5 for more details on splice joints.

- The length of the straight section of the coils was shortened by about 200 mm to accommodate the splice joints within the coil end-saddle and still use the present tooling.

- The two half-coils were separated in the reaction fixture using stainless steel plates. This allowed better control of the coil mid-plane and also gave the option of splicing each half coil separately.

- The first half-coil was impregnated separately and then the second half-coil was impregnated along with the already impregnated first half-coil. The first step ensured the correct midplane position and the second step ensured proper matching between the two half-coils.

[1] HFDA-03 Production Report, TD-01-064

- All the outer pole pieces except for one had no extensions. A separate extension was placed on top the outer pole pieces during assembly. This was done to ensure prestress symmetry between the left and right side of two half coils. Note that in the previous magnets the left and right sides of the coil assembly had different stresses due to misalignment of pole pieces during impregnation.

- The G-10 end splice support structure was optimized based on the fabrication experience of the first three magnets.

The following sections will outline the details of the magnet fabrication techniques and the data collected during magnet assembly.

2.0 STRAND and CABLE

OST using Modified Jelly Roll Process manufactured the conductor used for HFDA-04. The nominal diameter of the strand was 1.00 mm with an effective filament diameter of 115 μm. The Cu to non-Cu ratio was 0.92.

Rutherford type cable with 28 strands was manufactured at LBNL. Note the cable used in HFDA-04 does not have the stainless steel core unlike the previous magnets. The cable parameters are listed in Table 1. The cable was initially cleaned with ABZOL-VG to remove any oil residue left from the cabling process. It was then heat-treated at 200 ^{o}C for 30 min to reduce the residual twist in the cable that also comes from the cabling process.

Parameter	Unit	Value
Mid-Thickness	mm	1.7994
Width	mm	14.242
Keystone angle	deg	0.918
Pitch Length	mm	109.8
Number of Strands		28
Lay Direction		Left
Reel Number		782-B

Table 1: *Cable parameters as provided by LBNL.*

Four virgin and four extracted strand samples were placed as witness samples on the reaction fixture along with the coil assembly. The samples were placed along the length of the retort (one virgin and one extracted near LE and RE, two virgin and two extracted samples in the center of the coil) to understand if there is any variation in temperature. Table 2 lists the measurements made at the SSTF. Note that the measured data is lower than expected. This has been attributed to the expansion of the Ti-alloy barrels through oxygen absorption during reaction (see Fig. A1)[2]. Based on these measurements the short sample limit of the magnet is about 20 kA at 12 T.

[2] E. Barzi, personal communication

Sample #	Sample State	Sample Location	Ic (@ 12T) A	n	RRR
1	Virgin	RE	708	14	5
2	Virgin	Center	594	n/a	13
3	Virgin	Center	671	14	7
4	Virgin	LE	703	16	111
5	Extracted	RE	583	n/a	36
6	Extracted	Center	654	n/a	42
7	Extracted	Center	Quenched	n/a	4
8	Extracted	LE	Quenched	n/a	32

Table 2: *Measured critical parameters of the witness sample.*

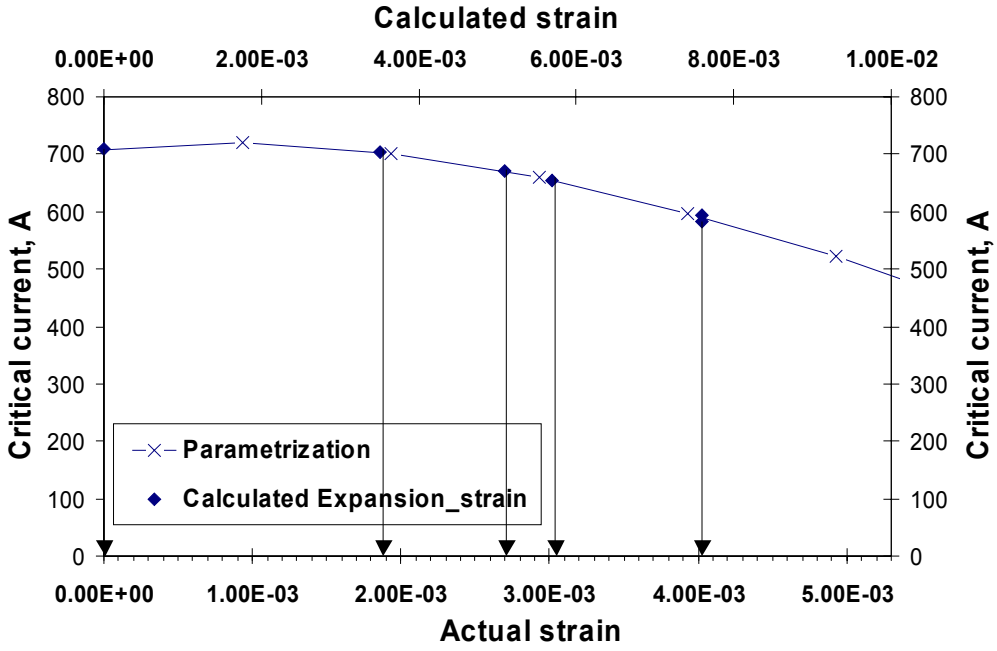

Fig. A1: *Effect of strain induced due to the Ti barrel expansion on the critical current.*

3.0 COIL FABRICATION

3.1 End – Saddle Design:

Both inner and outer layer end-saddles were redesigned such that the Nb_3Sn lead cable and the splice joints are better supported. The Nb_3Sn lead cable in the new design stays in the mid-plane and is always supported by the end-saddle, thus preventing any bending strain. The pre-tinned NbTi and Cu cables are placed on top of the Nb_3Sn lead cable. Note the in the previous design the lead cable was unsupported when it comes out of the saddle and before the splice joint begins. Furthermore in the new design the splice joint itself is embedded in the end-saddle thus providing support at all stages of magnet assembly. Note also that in the previous magnets, the

splice joint is outside the coil and 1/3 of its length is unsupported until impregnation. The following solid models should illustrate the above points –

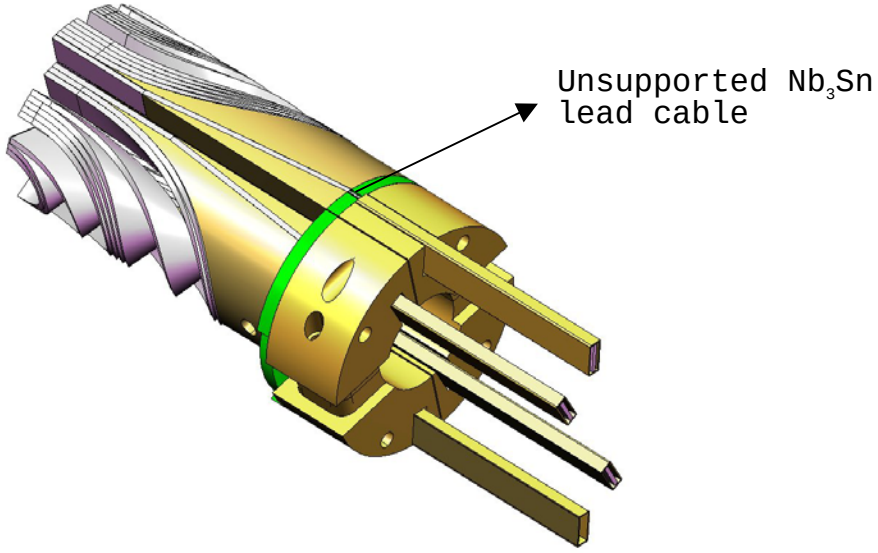

Fig. 2: *End – saddle and splice geometry in magnets, HFDA-02 and HFDA-03*

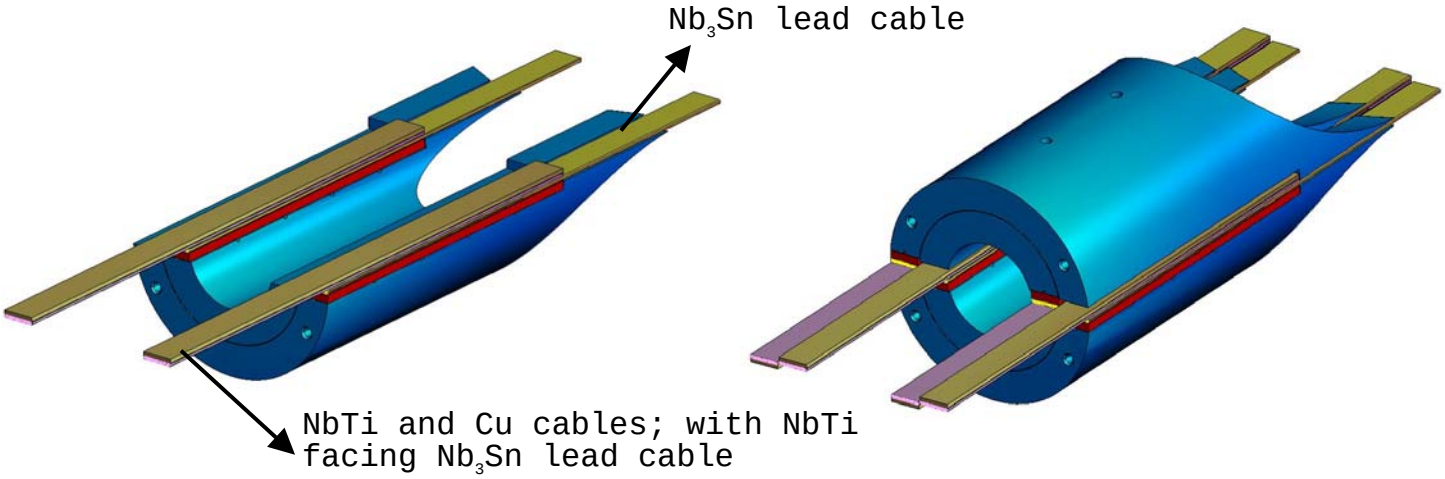

Fig. 3: *End-saddle and the splice geometry for the magnet, HFDA-04*

3.2 Coil Winding and Curing

Based on our studies concerning the cable thickness expansion during heat-treatment[3], the cable insulation thickness for the coils was adjusted. The percentage overlap of the insulation tape for both the cable and the wedges was 46%. Note that in HFDA-03 percentage overlap of the insulation for cable was 40% and for wedges it was butt lap. It was discovered during

[3] N. Andreev, E. Barzi, D. Chichili, S. Mattafiri and A. Zlobin, "Volume Expansion of Nb-Sn Strands and Cables During Heat-Treatment", CEC/ICMC01, Madison, WI July 01.

installation, that the outer layer end-spacers were about 15 mils oversized than the straight section pole pieces. So 15 mils of stainless steel shim was added between the straight section pole pieces and the outer layer first turn. Later after coil reaction these stainless steel shims were replaced with G-10 shims. The winding and curing procedure was similar to that of HFDA-03. Fig. 4 shows the two half coils wound and cured –

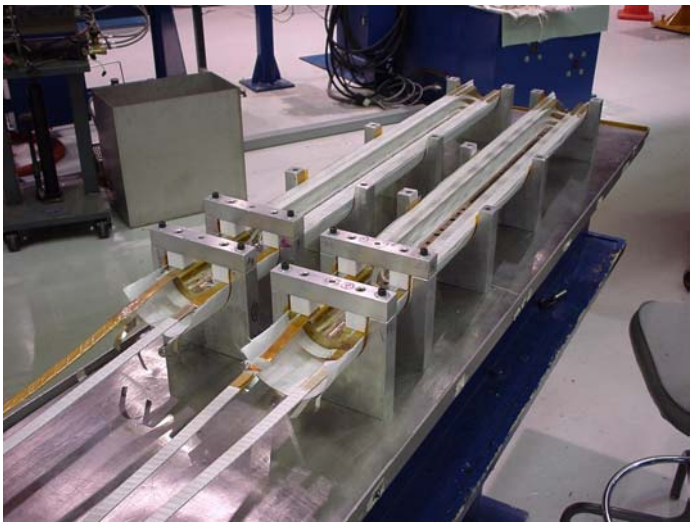

Fig. 4: *Cured Half Coils*

The inter-layer insulation consisted of two layers of ceramic cloth each 0.125 mm thick, while the ground insulation has three layers of ceramic cloth of each 0.125 mm thick. The middle layer of the ground insulation consists of the quench protection heaters (see HFDA-03 production report for a photograph). The heater-wiring diagram is also similar to that HFDA-03 and is shown in Fig. 5.

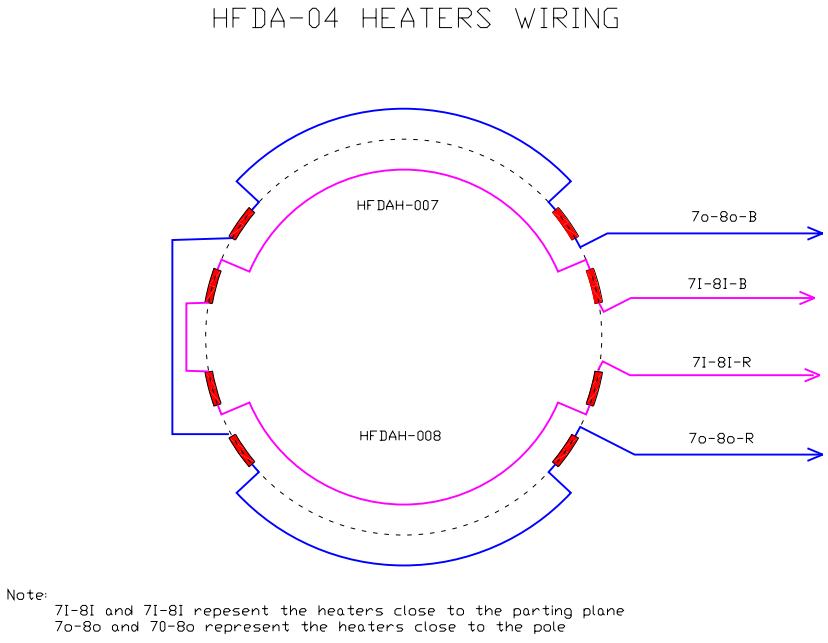

Fig. 5: *HFDA-04 heater wiring diagram*.

3.3 Coil Electrical and Mechanical Measurements:

Electrical measurements (L, Q and R) were taken on both the half coils before placing them into the reaction fixture to check for possible turn-to-turn shorts. The data is shown in Table 3. Both the coils have similar values and match the theoretical estimates, which indicate that the coils are free from turn-to-turn shorts. Note that the inductance, L and Q were measured at 1 kHz. Resistance was measured using four-wire technique at 0.1 A.

	Resistance mΩ	Inductance μH	Q
HFDAH-07	54.77	223.767	6.18
HFDAH-08	53.50	223.736	6.15

Table 3: *Electrical measurements on the cured half-coils.*

The azimuthal size in the straight section of the half-coil, HFDAH-007 was measured after low-temperature curing at two positions at varying pressures. Fig. 6 shows the data with respect to the nominal size. Note that these measurements were taken before the installation of the ground insulation. The mean azimuthal size of HFDAH-07 is about 1.00 mm below the nominal size, closed to the desired size. The azimuthal size of the second half-coil, HFDAH-08 was not measured.

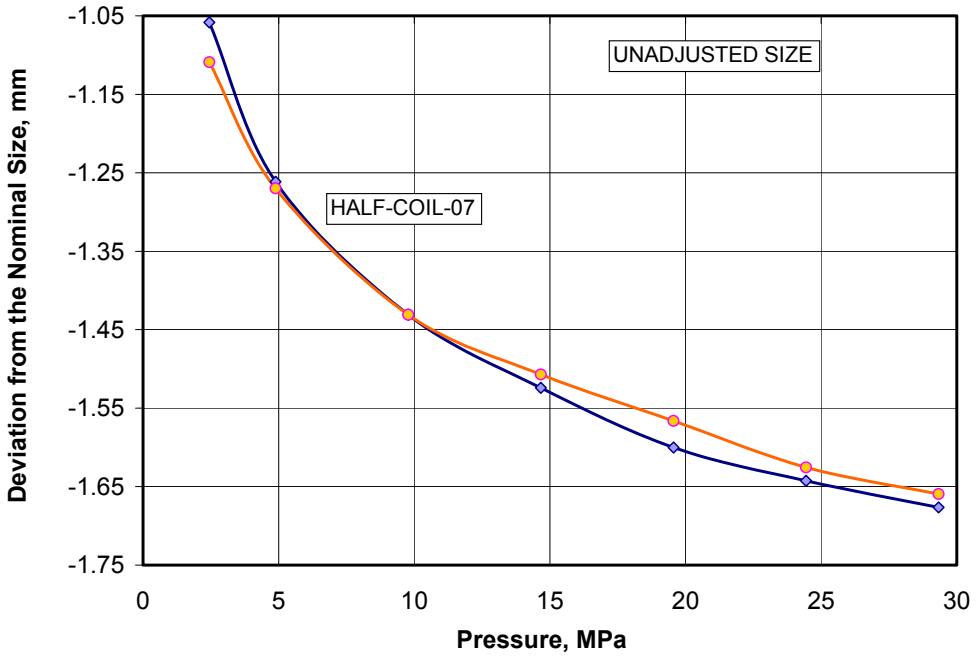

Fig. 6: *Azimuthal size of the half coil, HFDAH-007.*

4.0 COIL REACTION

The two half-coils were separated in the reaction fixture using stainless steel plates. Each half coil was fixed to one half of the reaction fixture using these spacers. This allows better control of the coil mid-plane and also has the option of splicing each half coil separately. Fig. 7 shows the assembled reaction fixture to be placed in the retort. Note that this time the lead cables were cut long and bent over the reaction fixture to reduce the effects of welding the cable ends.

The reaction cycle followed for HFDA-04 is similar to that of HFDA-03 and is given in Table 4. The two half-coils were assembled into the reaction fixture and then placed inside the retort. Since the coils were undersized, the two halves of the reaction fixture closed very easily. Two thermocouples were attached to the end saddles on either end to measure the temperature of coil and a third one was placed inside the retort to measure the temperature of the argon. The measured temperature profiles are shown in HFDA-02 production report [TD-01-036].

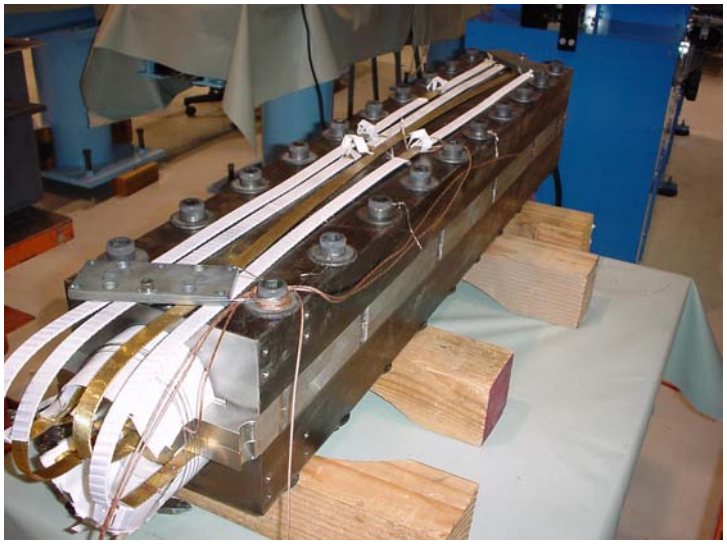

Fig. 7: *Coils assembled in the reaction fixture*

	Ramp Rate ^{o}C/hr	Temperature ^{o}C	Dwell Time hr
Step - 1	25	210	100
Step - 2	50	340	48
Step - 3	75	650	180

Table 4: *Heat-treatment cycle used in HFDA-04*.

5.0 SPLICE JOINTS

As mentioned earlier the end-saddles were redesigned to support the splice joints at all stages of the magnet assembly. Note that the entire length of the splice joint now sits inside the end-saddle

(see Fig. 3). To insulate the lead cable both electrically and thermally, a ceramic piece was placed between the end-saddle and the Nb_3Sn lead cable in the splice region. The red colored strip shown in Fig. 3 is the ceramic piece.

Several mock-up tests as shown in Fig. 8 were performed to adjust the tooling and to obtain the right parameters such as pressure, amount of solder strip and temperature for splicing procedure. Once the splicing procedure was obtained, electrical tests on splice joints were performed using a superconducting transformer. The detailed description of the transformer and the various tests performed are reported in two technical notes[4]. Tables 5 through 7 show some of the test results. The first two samples quenched due to mechanical strain induced during the splicing operation. With slight tooling modifications the motion of the Nb_3Sn cable was restricted and the samples tested after that did not quench. Note that the peak current reached as high as 22.5 kA and was limited by the system capability. The lower peak currents in some of the samples are due to higher splice resistance. The effect of pressure and the cable displacement on the splice current and/or splice resistance was also studied. These results show that the splicing technique is robust and repeatable.

For HFDA-04, the splice cables consist of one NbTi and one Cu cable with NbTi facing Nb_3Sn lead cable. Note that in the previous magnets we used two NbTi cables, one on each side of the Nb3Sn lead cable. The NbTi and Cu cables were first pre-tinned and soldered together before splicing them on to the Nb_3Sn lead cable.

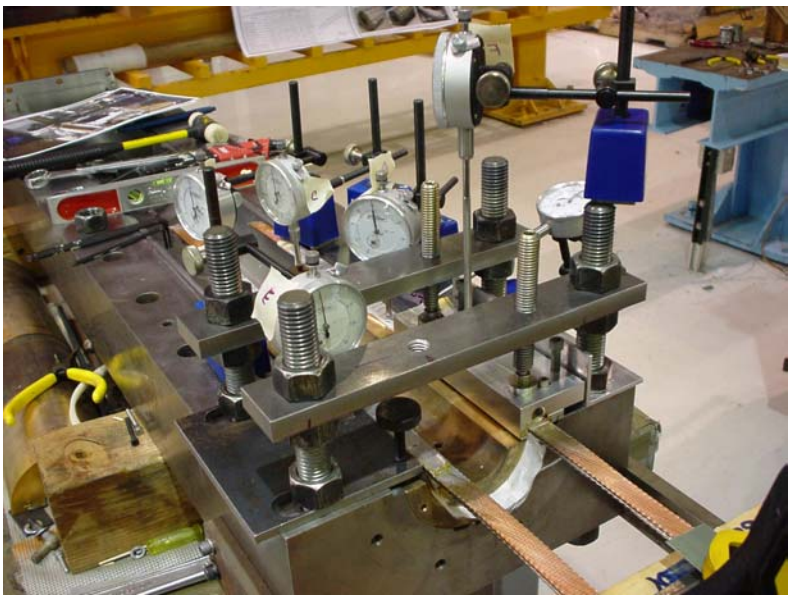

Fig. 8: *Mock-up tests to refine the splicing procedure*

[4] I. Terechkine et al., "SC Current Transformer for Testing Nb_3Sn Cable Splicing Technique", TD-02-014.
S. Bhashyam et al., "Results from Parametric Studies and Testing Splicing Technology Using Superconducting Current Transformer", TD-02-023.

Sample #	Splice Resistance nano-ohms	Current kA	Comments
1	6 (1 + 5)	13	Quenched. The reason is the mechanical strain induced in Nb_3Sn cable due to relaxation of NbTi cable.
2	2.5 (1.5 + 1)	16	Quenched. The cable might have been displaced during splicing. Acceptable splice resistance
3	5 (2 + 3)	19	No quench. Splice Tooling was modified. However, low pressure was applied during splicing operation which resulted in high splice resistance.
4	2.5	22.5	No quench. Good quality of splices with acceptable splice resistance. Pressure during splicing operation was increased.

Table 5: *Initial experiments to optimize the splicing procedure and tooling.*

Pressure MPa	Splice Thickness Deviation mm	Splice Resistance nano-ohms	Current* kA
2	0.625	2.2	16.5
5	0.500	1.7	18.6
9	0.375	1.4	20.5
23	0.250	1.2	21.5
38	N/A	1.1	21.8

Table 6: *Effect of transverse pressure on the splice resistance and current. *Note that none of samples quenched. The peak current reached was limited by the system.*

Splice Tip Displacement, mm	Displacement @ 7 mm from Clamp, mm	Current* kA	Splice Resistance nano-ohms
17 (out of cable plane)	0.250	19.5	1.6
4 (in the cable plane)	0.200	17.6	2.1

Table 7: *Effect of cable displacement on the current. *Note that none of samples quenched. The peak current reached was limited by the system.*

Figs. 9(a) and 9 (b) show the set up and the finished splice joints respectively on the half coil, HFDAH-007. The width and thickness dimensions of the splice joints are given in Table 8. A 5-mil thick Kapton cap was placed around the splice joint to insulate from surroundings. To save some real estate the 5-mil thick Kapton ground insulation, which was placed around the coil, was cut at the beginning of the splice joint and folded into the mid-plane, (see Fig. 10).

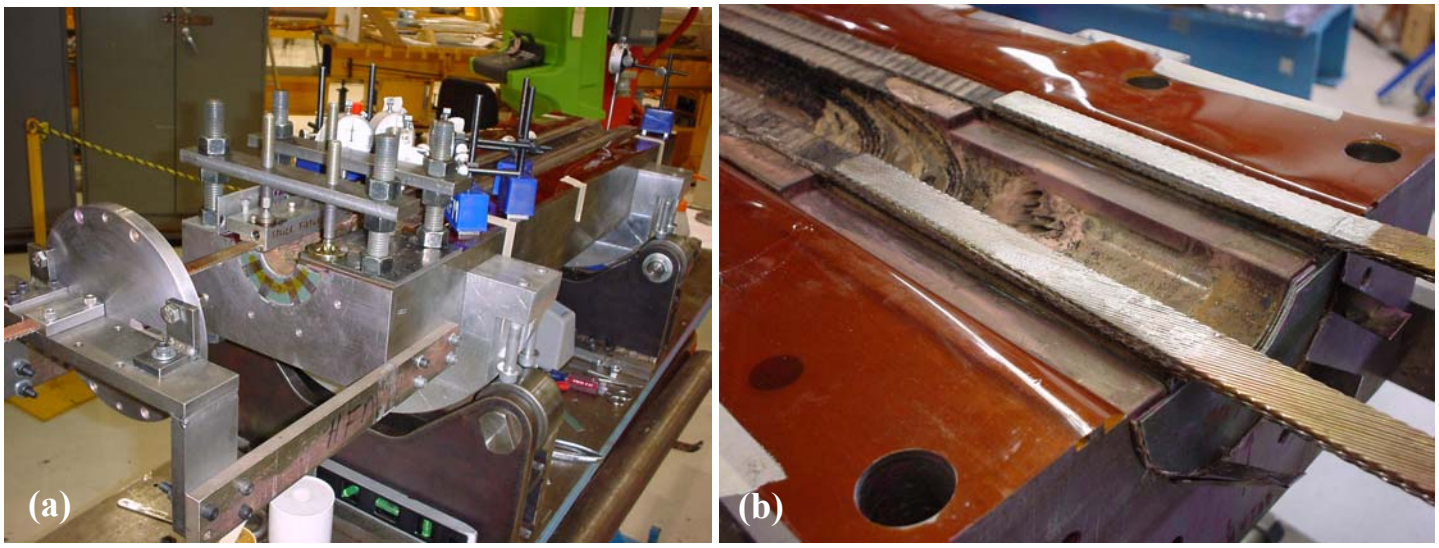

Fig. 9: *(a) Set up to make the splice joints (b) Finished splice joints on the half coil, HFDAH-007.*

	Nominal dimensions	*HFDAH-007*		*HFDAH-008*	
		Inner	Outer	Inner	Outer
Width, in	0.580	0.590	0.585	0.587	0.575
Thickness, in		n/a	n/a	0.149	0.148

Table 8: *Dimensions of the finished splice joints for the two half coils*

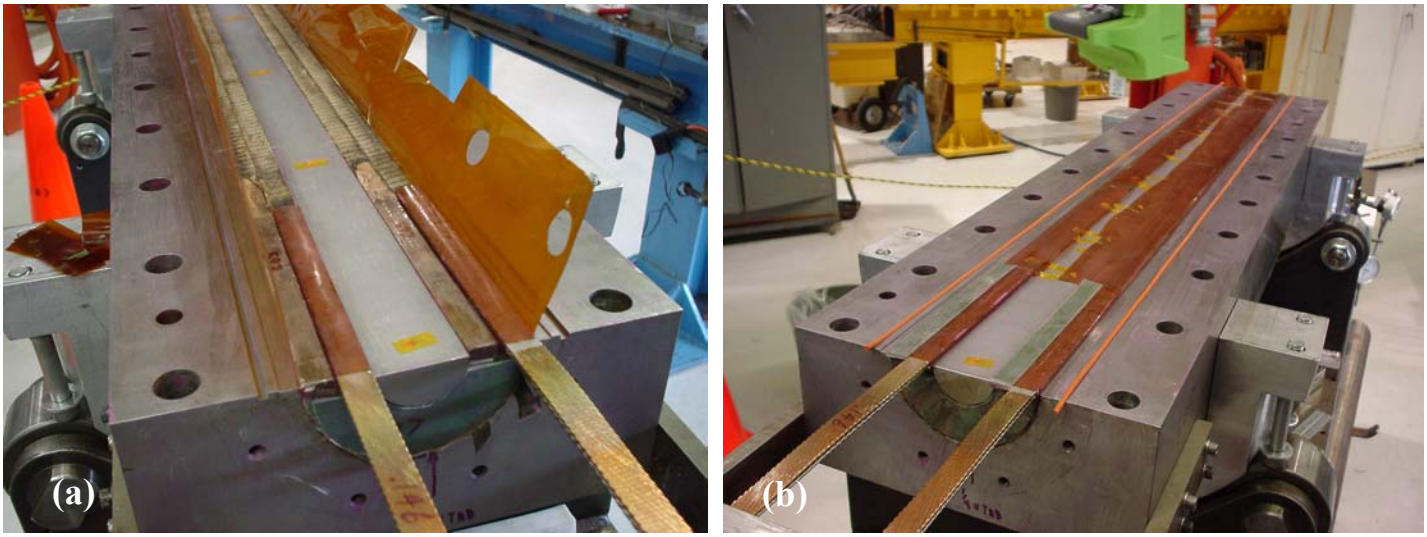

Fig. 10: *(a) Insulation around the splice joints (b) Kapton ground insulation*

6.0 EPOXY IMPREGNATION

The impregnation procedure for this magnet was changed to accommodate the changes in splicing procedure. Half coil, HFDAH-007 was impregnated separately after splicing. Note that the splicing operation was done in the impregnation fixture (see Fig. 10b). The half coil as shown

in Fig. 10 (b) is ready to be impregnated. The assembly was closed using a flat stainless steel plate with slots to accommodate the splice joints. The impregnation procedure was very similar to the previous magnets. Fig. 11 (a) shows the impregnated half coil. Fig. 11 (b) shows the voltage taps on the splice joint attached after impregnation.

The next step was to assemble the second half coil with the impregnated first half coil. This procedure would eliminate any mismatch in the mid-plane between the two half coils. **There was some difficulty in assembling the two half coils. The outer pole extension was rounded to gain some space.** Once the half coils were assembled, the impregnation process went smoothly. The height of the slots in the end-saddles was more than thickness of the splice joints, so the remaining gap was filed with G10 strips. Fig. 12 shows the impregnated coil assembly.

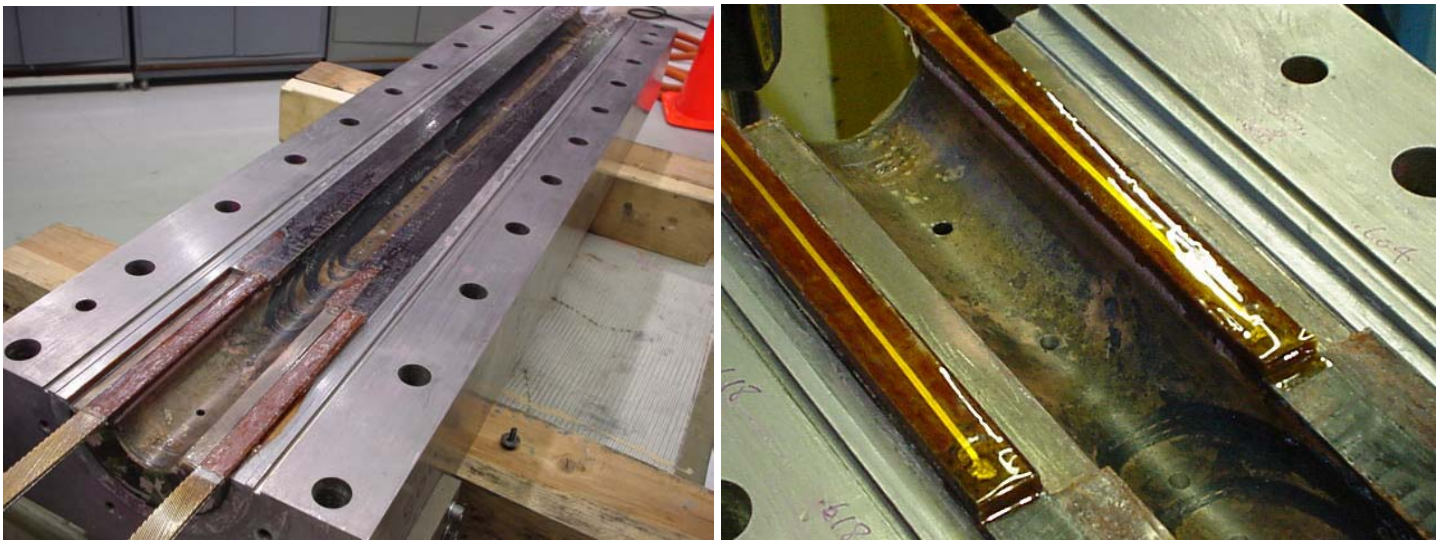

Fig. 11 *(a): Impregnated half coil (b) Voltage taps on the splice joint*

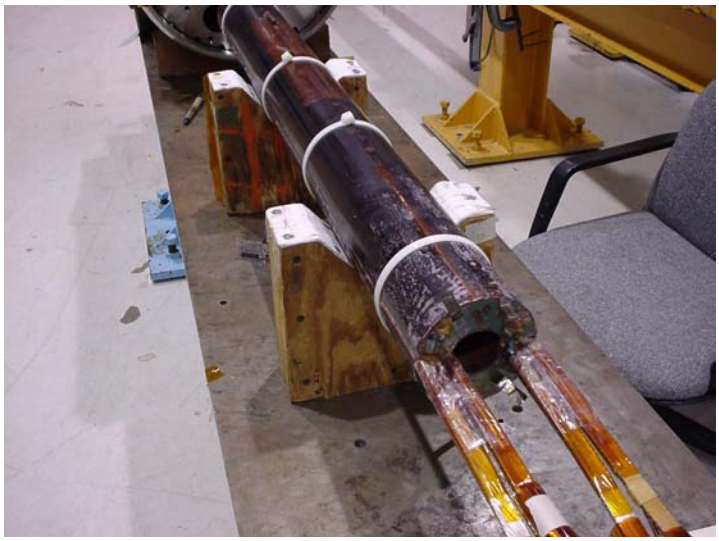

Fig. 12 *Impregnated coil assembly*

Electrical measurements (L, Q, and R) were performed on the impregnated coil assembly. Table 9 shows the data. For comparison measurements taken before reaction were also included in the table. The resistance of the coil assembly after reaction increased by about 70%. The Q decreased by the same amount as the inductance of the coil remained constant before and after reaction. Most importantly the two coils have similar values, which indicate that there are no turn-to-turn shorts. Note that L and Q are measured at 1 kHz and the resistance measurements were done at 0.1 A using four wire measuring technique.

Hi-Pot tests up to 1 kV were also performed on the impregnated coil assembly to check current leakage between coil-to-coil, coil-to-ground, coil-to-heaters and heater-to-ground. The current was less than 0.04 μA at 1 kV.

Parameter	Before Reaction		After Reaction and Impregnation	
	HFDAH-07	**HFDAH-08**	**HFDAH-07**	**HFDAH-08**
Resistance, mΩ	54.77	53.60	92.77	92.98
Inductance, μH	223.77	223.74	208.93	210.08
Quality Factor	6.18	6.15	2.13	2.13

Table 9: *Electrical measurements of coil @ 1kHz after reaction and impregnation.*

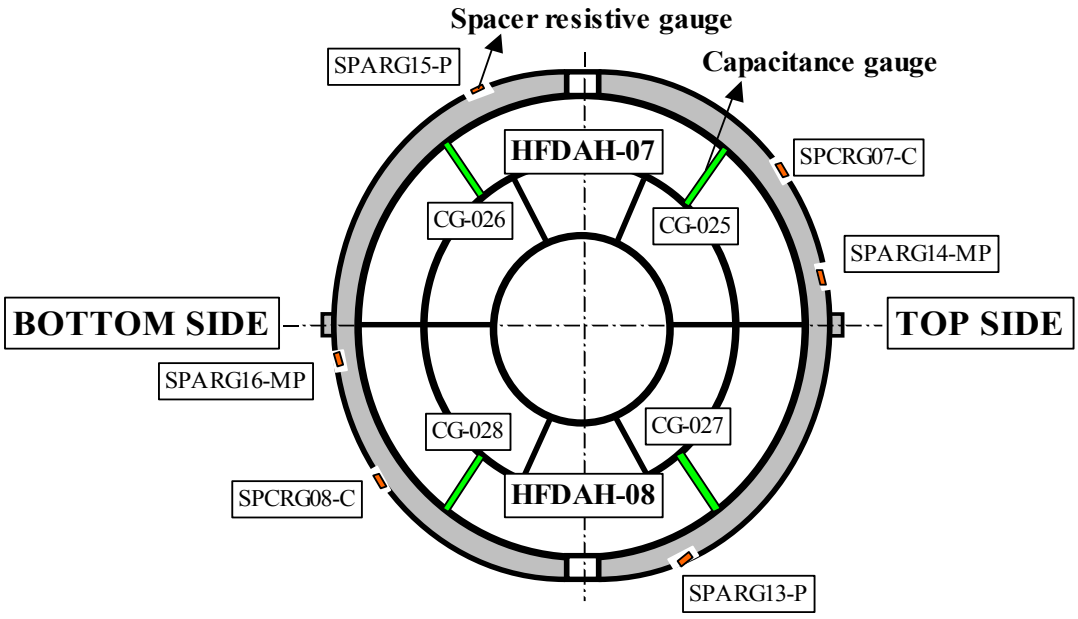

Fig. 13: *Instrumentation layout in the straight section of the magnet*

7.0 INSTRUMENTATION

One outer pole piece on each half-coil was mold released before epoxy impregnation so that they can be removed after impregnation. Two outer pole pieces were modified to accept capacitance

gauges and were placed at these locations. Resistive gauges were mounted on the circumferential grooves made on the aluminum spacers. Fig 13 shows the layout of gauges in the magnet cross-section. The capacitance gauges measure the azimuthal stress in the outer layer of the half-coils while the resistive gauges measure the azimuthal stress in the aluminum spacers. In order to estimate the stress distribution near the splice joint, the last Aluminum spacer both on the top and bottom side were also instrumented with resistive gauges.

8.0 YOKING

The impregnated coil assembly was measured to be 50 μm under the nominal size. Furthermore, to account for the reduction in size during the first massaging cycle, 75 μm thick Kapton shim was placed around the coil straight section and 50 μm thick in the ends.

The coil assembly procedure into the yoke assembly was similar to that of the previous magnets. The pump pressure was increased in 1000 Psi increments and the gauge readings were recorded. Unlike the previous magnets, the loading was quite symmetric between the left and right half coils. It's partly due to the fact that we have floating pole extensions all along the length of the magnet. Figs. 14 and 15 show the evolution of stress in the coil and in the spacers during the initial loading cycles. The azimuthal stress in the coil was higher than predicted by analysis. Note that in the previous magnets we also added shims along the pole extension to get symmetrical loading. This increased the interference between the spacer and the pole extension and thereby reduced the transfer of the stress to the coil. In this magnet we added the radial shim according the results from the previous magnet without accounting for the reduction in the interference between the spacer and the pole extension, thereby increasing the stress in the coils. However, after determining that the coil stresses will not reach more than 150 MPa at any stage of the magnet operation by performing the analysis with no azimuthal interference between the spacer and pole extension we proceeded with the magnet fabrication. Note that during the entire loading operation, 50 mil thick stainless steel shims were placed between the top and bottom stainless steel yoke pieces not to over compress the ends and especially the Nb_3Sn lead cable and splice joints in LE.

At 8000 pump Psi, the gap between the yoke halves was close to the nominal value and the clamps were inserted using a separate set of pusher blocks. Two clamps, one on each side were inserted simultaneously starting from the middle of the magnet. Note that during the entire operation the coil resistance was monitored to make sure we do not have any turn-to-turn shorts. Table 10 gives the data during yoking operation. Note that after spring-back, the azimuthal stress in the outer layer of the coil is about 45 MPa compared to 20 MPa predicted by analysis. As stated earlier this increase in stress is due to reduced interference between the spacer and the pole extension. This can also be inferred from the fact that the stress in the spacer pole region after spring-back is small compared to ANSYS calculations with nominal dimensions.

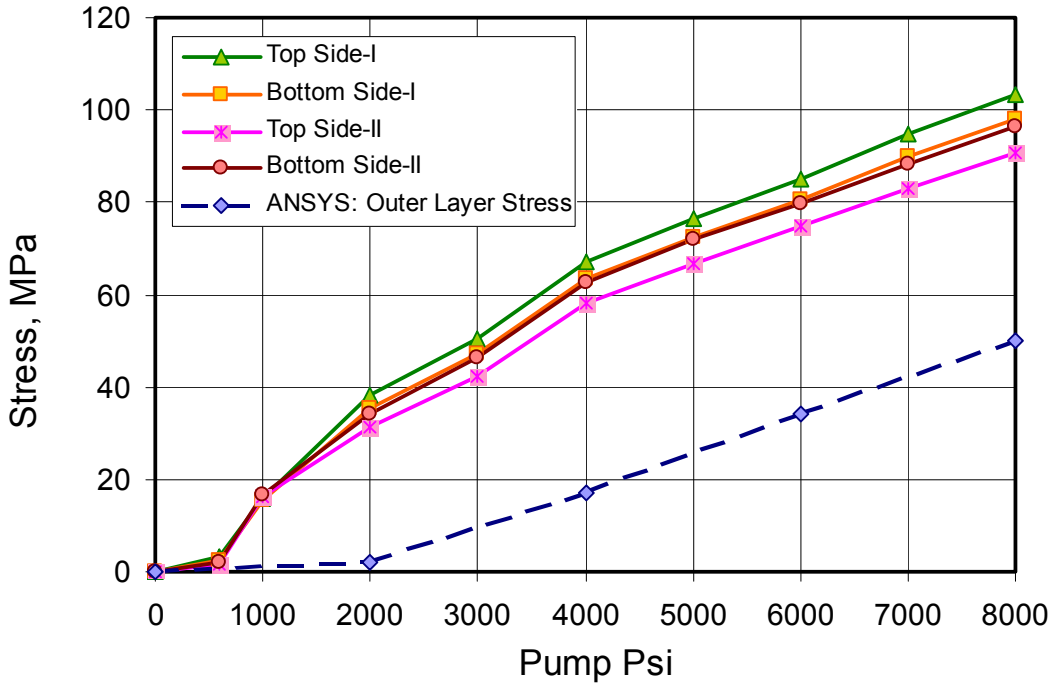

Fig. 14: *Evolution of azimuthal stress in the coil outer layer during yoking operation*

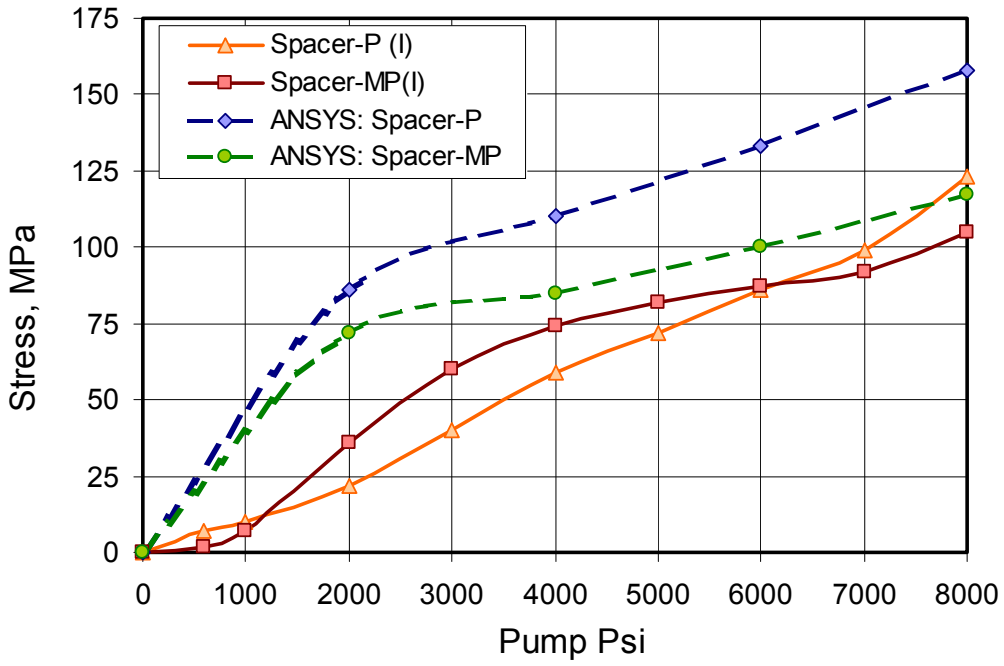

Fig. 15: *Evolution of azimuthal stress in the spacers during yoking operation*

HFDA-04	UNDER PRESS MPa		DURING CLAMPING MPa	AFTER SPRING BACK MPa		AFTER WELDING SKIN MPa	
	Data	ANSYS	Data	Data	ANSYS	Data	ANSYS
COIL OUTER LAYER	96	50	108	45	20	76	60
SPACER-POLE	112	160	137	50	108	91	165
SPACER-MIDPLANE	99	118	109	87	84	99	117
SKIN						~225	216

Table 10: *Summary of data collected during yoking and skinning*

9.0 SKIN AND END-PLATE INSTALLATION

The next step in the magnet assembly was to weld the two skin halves on to the yoked assembly. First the skin alignment keys were inserted into the grooves provided in the aluminum clamps. The whole assembly is then gently placed in the lower half of the skin that is already installed in the welding press. The upper half of the skin is then installed on the magnet. The two skin halves were compressed at 600 pump Psi during welding operation. After each weld pass, the distance between the top and bottom pushers was measured to compute weld shrinkage. Simultaneously the gauge readings were recorded to monitor the increase in coil stress with weld shrinkage. Figs. 16 and 18 shows the evolution of stress in the coil and spacers with the weld shrinkage. The stress in the skin was also monitored during welding operation. The mean azimuthal stress in the skin exceeded the yield limit, which is about 225 MPa.

After welding, the ends of the skins were cut to the right dimensions. The end plates were then welded on both lead and return ends to provide axial support to the coils. Finally the twist along the length of the magnet was measured using twist-measuring device. Fig. 18 shows the variation of the twist along the length of the magnet. On average the twist is about 1.7 milli-radians per meter. Six gauges were installed along the length of the skin to measure the longitudinal stress in the skin during excitation.

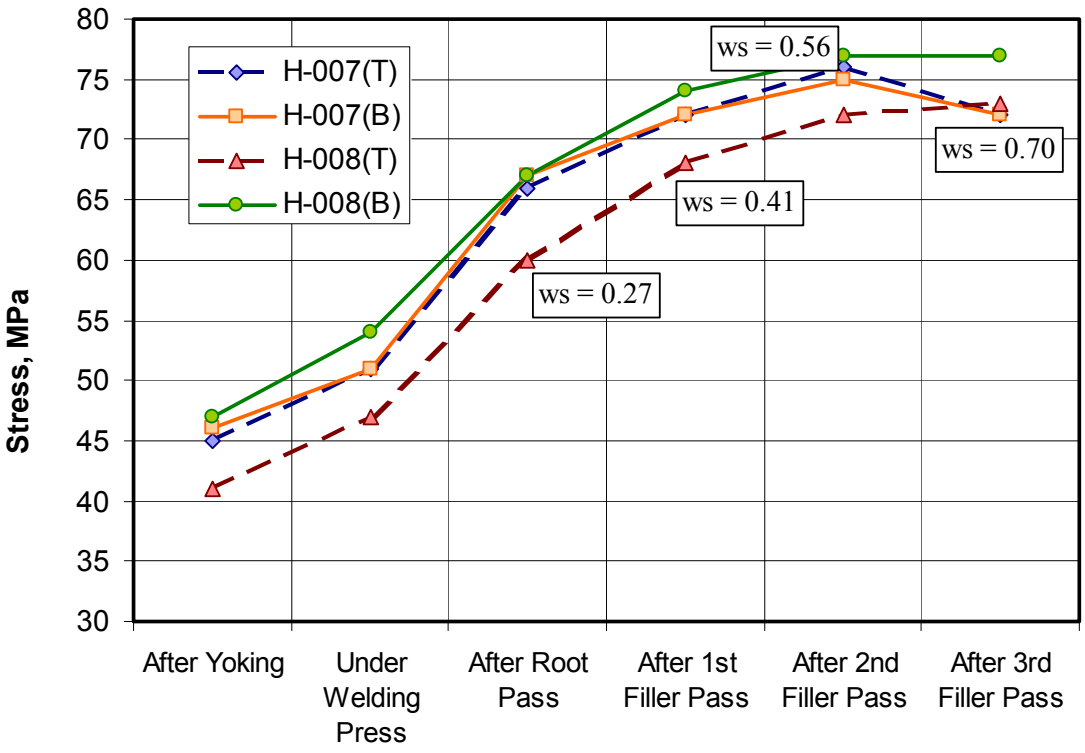

Fig. 16: *Evolution of coil azimuthal stress with weld shrinkage.*

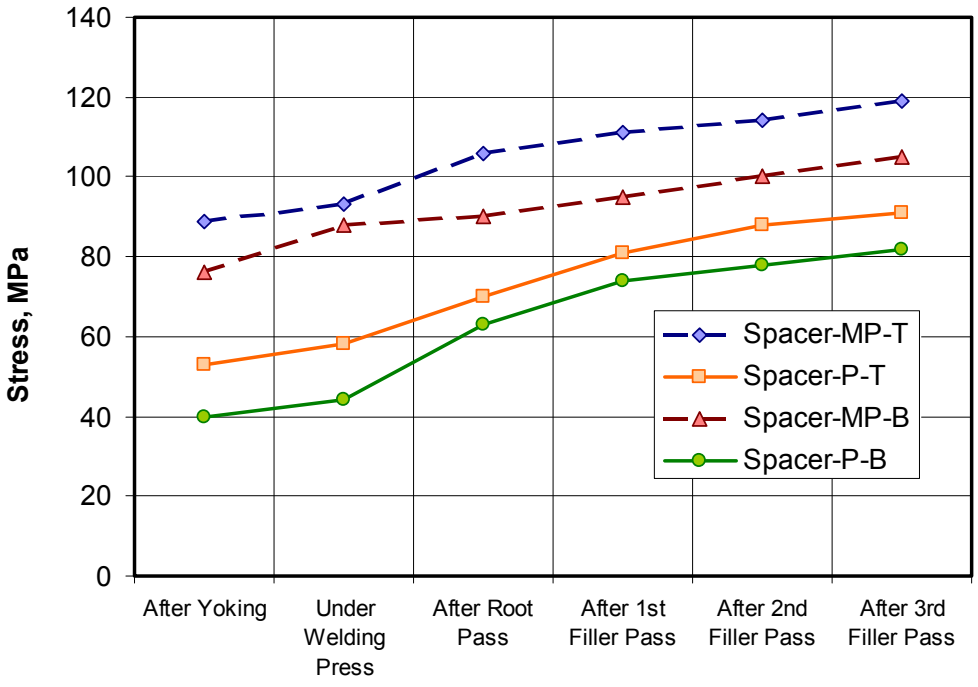

Fig. 17: *Evolution of spacer azimuthal stress with weld shrinkage.*

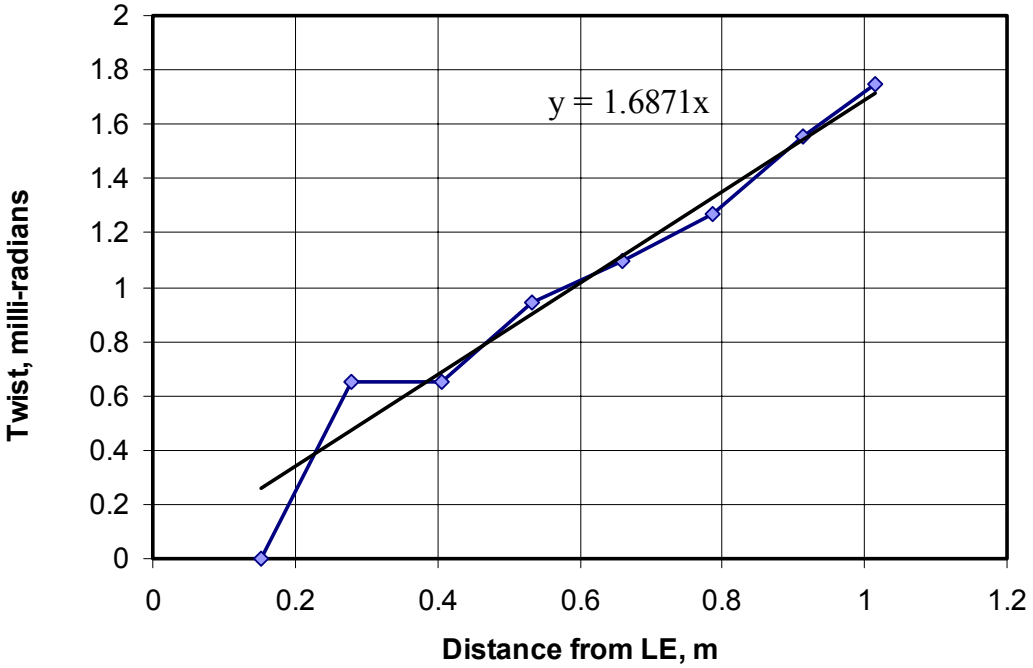

Fig. 18: *Variation of twist along the length of the magnet.*

10.0 FINAL ASSEMBLY

Once the end plates were welded, the bullets were installed on both LE and RE. Four bullets per end were torqued until each bullet sees 500 lbs of force. Note that the bullets were installed with strain gauges and were calibrated both warm and cold.

The last mechanical assembly involved performing the half-coil splices. The outer layer leads from both the half-coils were spliced together and captured in a G-10 box. The inner layer leads were used as power leads for the magnet. The half-coil splice assembly was achieved without fixing the leads using "green putty" to the G-10 spacers. This would enable the leads to move under Lorentz forces if necessary.

Several voltage taps were installed on the lead cables before installing the splice box assembly as per drawing MB-411080 (Fig. 19). All the wires were finally terminated into hypertronic connectors to be hooked up in VMTF.

Electrical measurements were performed on the magnet just before shipping it to the VMTF. Table 11 summarizes these measurements.

	Resistance $m\Omega$	Inductance, mH		Quality Factor	
		At 1 kHz	At 20 Hz	At 1 kHz	At 20 Hz
HFDAH-07	89.63	0.112	0.336	1.17	0.18
HFDAH-08	89.94	0.113	0.337	1.18	0.18
Total Magnet	180.03	0.297	1.056	1.35	0.58

Table 11: *Electrical measurements on the half-coils and the total magnet*.

Fore reference, Fig. 20 shows the longitudinal cross-section of the magnet.

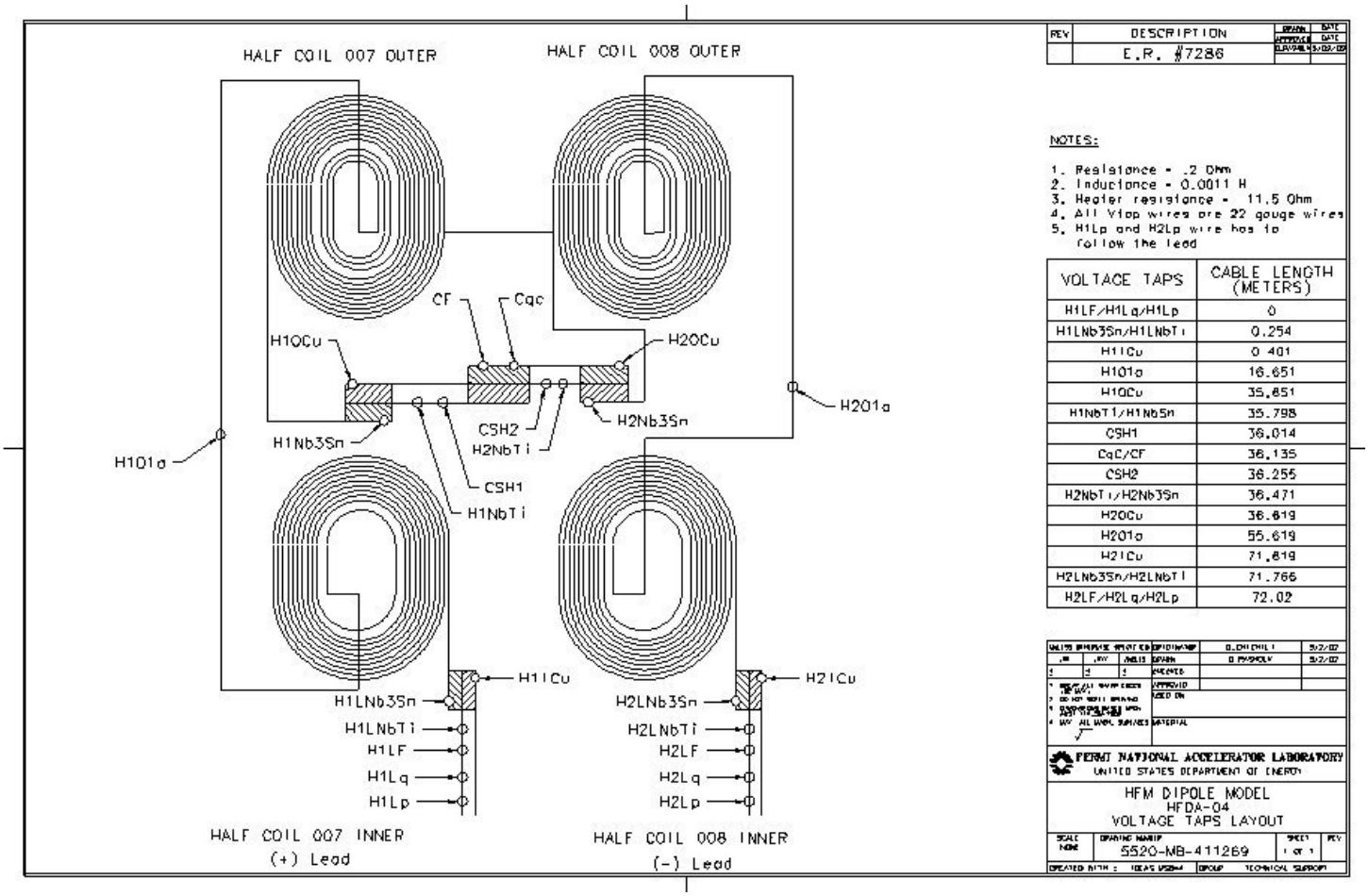

Fig. 19: *HFDA-04 voltage tap layout*

11.0 SUMMARY

The fourth shell-type Nb_3Sn high field dipole magnet, HFDA-04 was delivered to VMTF for testing on May 15, 2002.

The coil end-saddle was completely redesigned so that the lead cable comes in the mid-plane and the splice joint is within the end-saddle. This modification provided support to both the lead cable and the splice joint. Note that the total length of the straight section of the magnet was reduced by about 200 mm to accommodate the splice joint within the end-saddle and still use the present tooling.

We had some difficulty during assembly of the two half-coils after performing the splice joints. This issue is being investigated. For the next magnet, the NbTi and Cu cables will have smaller width there by making it easier to assemble the coils.

The stress in the coils was slightly higher than nominal and correspondingly the stresses in the spacer were lower than nominal due to decrease in interference between the spacer and the pole extension. This will be controlled in the future magnets.

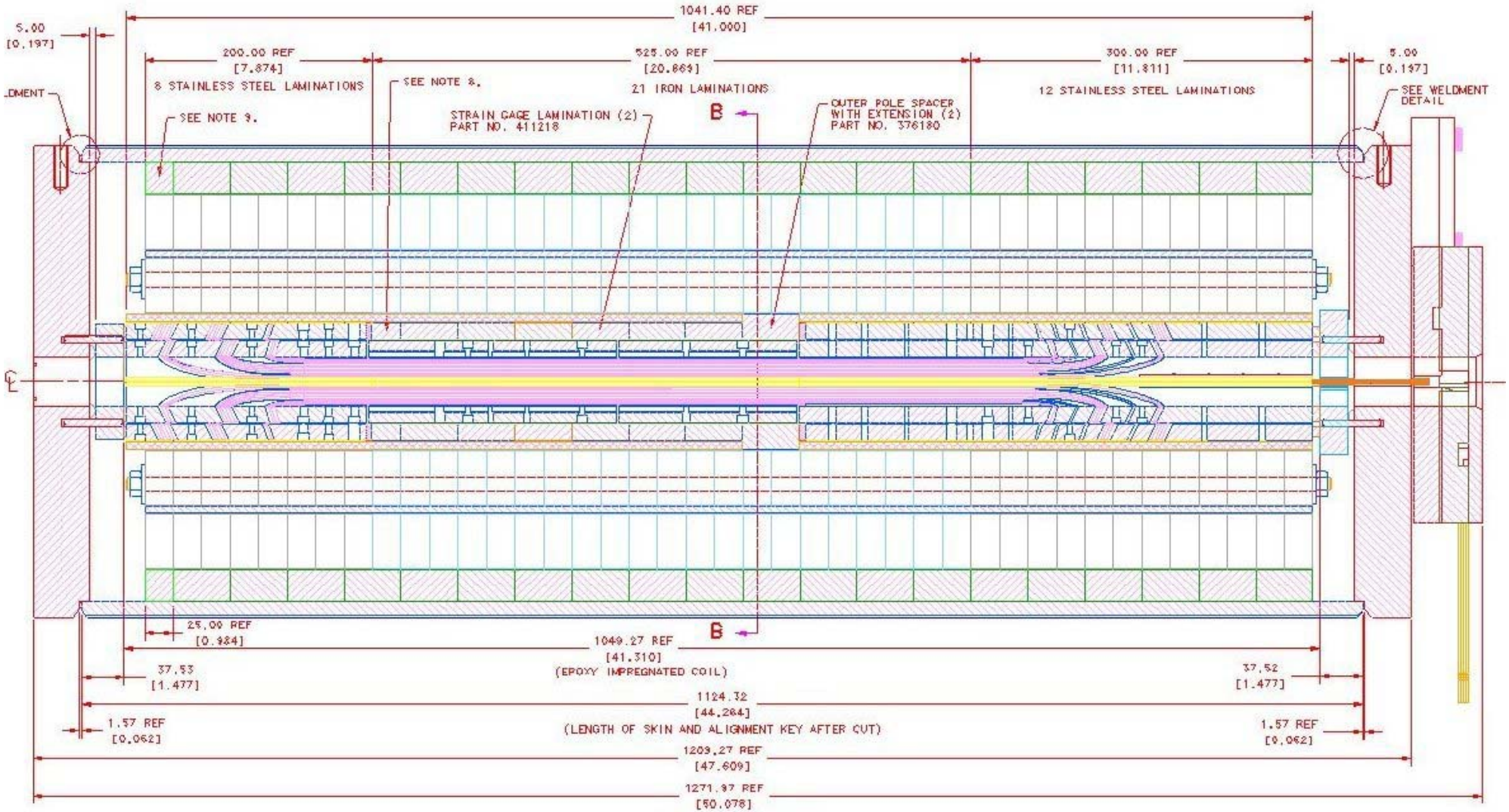

Fig. 20: *Longitudinal cross-section of HFDA-04*